

# A new fracture permeability model of CBM reservoir with high-dip angle in the southern Junggar Basin, NW China

*Energy Exploration & Exploitation*

2019, Vol. 37(1) 125–143

© The Author(s) 2018

DOI: 10.1177/0144598718807552

journals.sagepub.com/home/eea



Shiyu Yang<sup>1,2</sup>, Yidong Cai<sup>1,2</sup> , Ren Wei<sup>1,2</sup> and Yingfang Zhou<sup>3</sup>

## Abstract

Predicting the permeability of coalbed methane (CBM) reservoirs is significant for coalbed methane exploration and coalbed methane development. In this work, a new fracture permeability model of coalbed methane reservoir with high-dip angle in the southern Junggar Basin, NW China is established based on the Poiseuille and Darcy laws. The fracture porosity in coalbed methane reservoir is calculated by applying 3D finite element method. The formation cementing index  $m$  was calculated by combining fractal theory and the data of acoustic logging, compensated neutron logging, and density logging with the space method. Based on Poiseuille and Darcy laws, the curvature  $\tau$  is introduced to derive this new method for obtaining the permeability of the original fractures in coalbed methane reservoirs. Moreover, this newly established permeability model is compared with the permeability from the well testing, which shows a very good correlation between them. This model comprehensively includes the effects of fracture porosity, reservoir pore structure, and development conditions on fracture permeability. Finally, the permeability prediction of coalbed methane reservoir with high-dip angle in the southern Junggar Basin, NW China is conducted, which correlates very well with the well test permeability ( $R^2 = 0.83$ ). Therefore, this model can be used to accurately predict the coalbed methane reservoir permeability of low rank coals in the southern Junggar Basin. The permeability of the No.43 coalbed methane reservoir for the coalbed methane wells without well testing data is evaluated, which ranges from 0.000251 to 0.379632 mD. This significant change in permeability may indicate a complex coalbed methane reservoir structure in the southern Junggar Basin, NW China.

<sup>1</sup>School of Energy Resources, China University of Geosciences, Beijing, China

<sup>2</sup>Coal Reservoir Laboratory of National Engineering Research Center of CBM Development & Utilization, School of Energy Resources, China University of Geosciences, Beijing, China

<sup>3</sup>School of Engineering, Fraser Noble Building, King's College, University of Aberdeen, Aberdeen, UK

## Corresponding author:

Yidong Cai, China University of Geosciences, No.29 Xueyuan Road, Haidian District, Beijing 100083, China.

Email: yidong.cai@cugb.edu.cn



## Keywords

Permeability model, CBM reservoir, fractal dimension, logging data, southern Junggar Basin

## Introduction

Coalbed methane (CBM) is favorable for energy support, environmental protection, and mining safety (Cai et al., 2011; Karacan et al., 2008, 2011). The SJB covers an area of  $230 \times 50 \text{ km}^2$ , which located at the northern Xinjiang Uygur Autonomous Region, NW China. The major coal-bearing intervals are the Badaowan Formation (J1b) and the Xishanyao Formation (J2x). The vitrinite reflectance is of 0.38%–0.7%  $R_{o,m}$ , which belongs to the low-rank coal. The CBM reservoir properties are relatively poor, with permeability of 0.002–1.220 mD and porosity of 0.56%–9.73% (Chen et al., 2006, 2017; Fu et al., 2016; Li et al., 2017; Yin, 2009). Petrophysical properties including permeability, cementation factor, and porosity of CBM reservoirs have crucial impacts on CBM exploration and development (Li, 2016; Clarkson et al., 2011). Permeability of CBM reservoir is one of the key factors for evaluating CBM productivity. Many literatures related to permeability mainly emphasize the primary CBM reservoir permeability (Espinoza et al., 2014; Shovkun and Espinoza, 2017), dynamic permeability (Connell et al., 2016; Espinoza et al., 2015; Gentzis et al., 2009) and the relative gas/water permeability during gas production (Clarkson et al., 2011; Connell, 2016; Gensterblum et al., 2014).

Laboratory measurements, numerical simulation by production data, well injection/off tests, and geophysical logging methods can be used to evaluate the CBM reservoir permeability (Chatterjee and Paul, 2013; Mitra et al., 2012). The well logging may provide an economic and convenient way to acquire the CBM reservoir permeability (Saboorian et al., 2015; Zhou and Ya, 2014). However, a reliable permeability estimation model is firstly required to accurately evaluate the CBM reservoir permeability by the geophysical logging data. Multiple models of CBM reservoir permeability were established by using the well logging data of resistivity, density, gamma, and acoustic time (Chatterjee and Pal, 2010; Chatterjee and Paul, 2013; Saboorian et al., 2015; Yang et al., 2006; Zhou and Ya, 2014). However, these models have limitations for the specific high-dip CBM reservoir in the Hedong area of the SJB. Coal, as a typical dual porous material, includes matrix pores and fractures (Cai et al., 2013). Fracture performance determines the initial CBM reservoir permeability (Connell et al., 2016). Fracture permeability correlates with compensated density logging, shallow lateral resistivity logging (LLS), deep lateral resistivity logging (LLD), microsphere focusing logging data (MSFL), and the conductivity difference values of MSFL-LLD, MSFL-LLS, and LLS-LLD with the use of cluster and correlation analysis. The dual laterolog resistivity logging (LLS and LLD) is the well-established method to evaluate fracture permeability (Saboorian et al., 2015).

Many fracture permeability models were established with different fracture performance (Li et al., 2011), for instance, the three ideal fracture models of sheet, matchstick, and cube shape. A 3D finite element method to establish a fracture porosity calculation model has been discussed by many scholars (Cai et al., 2014; Martin and Malone, 2017). However, the general model to accurately describe the fracture complexity is difficult. Additionally, the fractures in the high rank coals ( $R_{o,m} > 2.5\%$ ) may be compacted by the overlying compressive stress. The fracture width can effectively constrain the CBM reservoir permeability

(Levine, 1996). Recently, the fractal theory was applied to evaluate the fracture complexity through the analysis of well logging data (Kundu et al., 2016; Masoumi et al., 2017; Ruspini et al., 2017; Yan et al., 2017; Zheng and Li, 2015).

In this paper, a new model for fracture permeability in a CBM reservoir will be established with the combination of the  $m$  value (formation cementation index) and the fracture porosity and the total porosity of the coal reservoir through the 3D finite element method. Then, the cementation index  $m$  value of CBM reservoir was detailed evaluated by the fractal dimensions from the well logging of acoustic logging (AC), compensated neutron logging (CNL), and density logging (DEN). Finally, the predicted permeability will be calculated with the established fracture permeability model, which compares with the permeability results from the actual well test.

## Geological background

The study area is located in the eastern part of the SJB. The southern Junggar Basin (SJB) covers an area of  $\sim 30,000 \text{ km}^2$ , which belongs to the foothills of the northern Tianshan Mountains and the eastern uplift. Due to the Himalayan movement, a series of large-scale thrust faults and a large number of pressure-torsional geological structures were developed. With the formation of large-scale fault structures, many secondary faults have been developed in the study area. Along the margin of the SJB, the anticline belts are developed from north to south, namely the Hutubi-Anji-West lake anticlines, the Huo-Ma-Tep backslope, and the piedmont belt. The anticline structures are closely associated with CBM exploration in the SJB, which include the Fukang, Toutun River, Changji, Karaza, Qigu, and Nankangkang anticlines. The structure of coal-bearing strata in the east is more complex than in the west (Chen et al., 2017). The high-dip anticline and fault structures developed in the Hedong area of the SJB, which provides favorable conditions for the CBM accumulation locally. This study is mainly aimed at the coal seams of No.43 and No.45 of Xishanyao Formation in SJB, and explores the original fracture permeability model of the main coal seam (Figure 1).

## Establishment of high-dip fracture permeability model

### Model derivation

In this work, fluid flow in a complex fracture in real CBM reservoir is assumed to be equivalent to fluid flow in a single fracture (Figure 2). The CBM reservoir is set to be a cube with side length  $L=1$ , the fracture length  $L_a$  and the fracture aperture  $b$ . The inlet pressure of the fluid through the fracture is  $p_1$ , and the outlet pressure is  $p_2$ .

Generally, the fluid flow in the fractures of CBM reservoirs satisfies the Darcy's law

$$Q = \frac{Ak(p_1 - p_2)}{\mu L} \quad (1)$$

where  $p_1$  and  $p_2$  are the pressures at the inlet and outlet of the fluid;  $A$  is the cross-sectional area of the coal;  $L$  is the model length of the coal;  $\mu$  is the viscosity of the fluid;  $Q$  is the flow rate and  $K$  is fracture permeability.

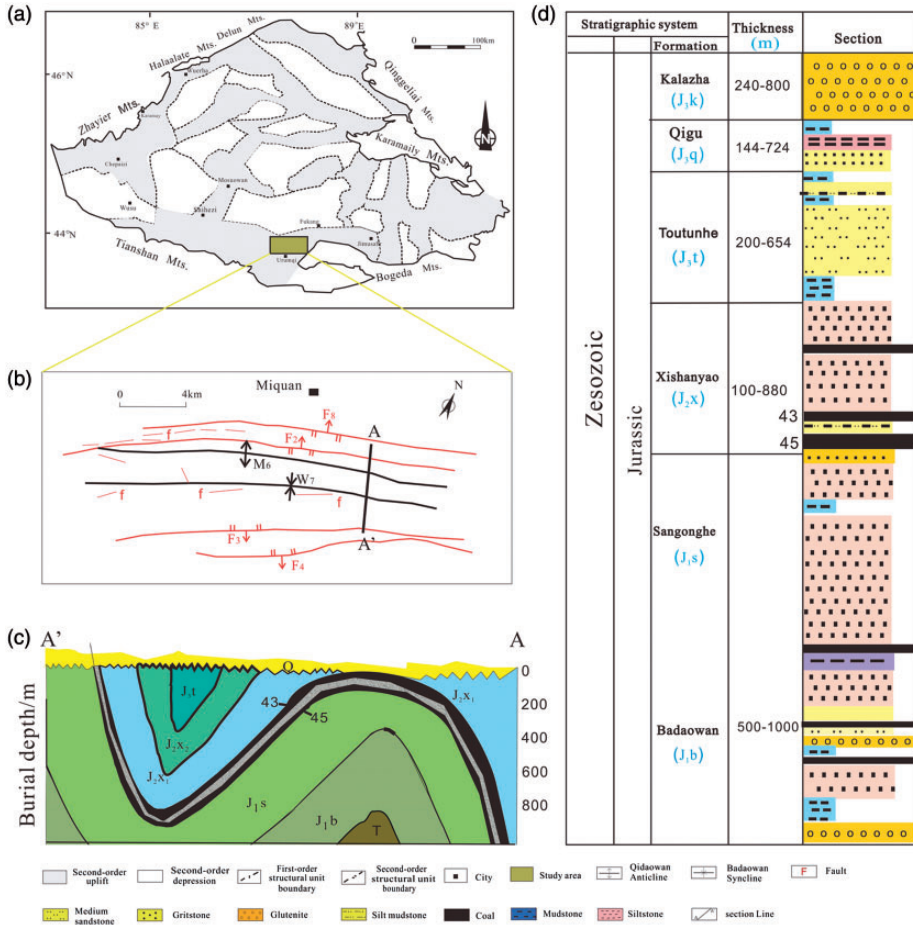


**Figure 1.** (a) Location map of study areas in the Junggar Basin, (b) structure outline map of Urumqi Hedong, stratigraphic distribution characteristics, (c) distribution of main coal seam, (d) column of a Jurassic stratigraphic section in the southern Junggar Basin; the target strata of CBM in the Xishanyao Formation strata are presented. CBM: coalbed methane.

According to Poiseuille’s law, the flow of fluid through a single fracture is

$$Q = \frac{b^3 La(p_1 - p_2)}{12\mu L} \tag{2}$$

where  $b$  is the fracture aperture;  $La$  is the distance the fluid flows.

Substituting equation (2) into equation (1), the fracture permeability can be rewritten as

$$k = \frac{b^3 La}{12A} \tag{3}$$

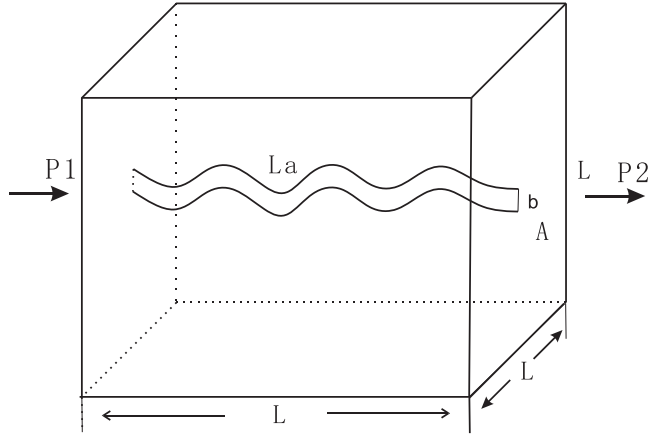


**Figure 2.** Schematic diagram of fracture system of coal reservoir.

When the flow path becomes tortuous, the flow through will be reduced. Therefore, the influence of the fracture buckling on the flow process needs to be considered. The equation (3) can be substituted as

$$k = \frac{b^3 La}{12A} \frac{1}{\tau} \tag{4}$$

where  $\tau$  is the tortuosity of coal fractures.  $\tau$  is defined as the square of the ratio of the travel length  $La$  of the fluid flow through the length  $L$  of the actual CBM reservoir (Wyllie and Spangler, 1952). Here,  $\tau$  is described as

$$\tau = \left(\frac{La}{L}\right)^2 \tag{5}$$

Substituting equation (5) into equation (4), the fracture permeability can be replaced by

$$k = \frac{b^3}{12La} \tag{6}$$

Winsauer and Shearin (1952) established the relationship between  $\tau$  and formation factor  $F$

$$\tau = (F\phi)^2 \tag{7}$$

The formation factor  $F$  in CBM reservoirs can be described by Archie formula

$$F = \frac{a}{\phi^m} \tag{8}$$

where  $a$  is the lithology index;  $m$  is the formation cementation index.

Substituting equations (7) and (8) into equation (4),  $L_a$  can be written as

$$L_a = \frac{a \cdot L}{\varphi^{m-1}} \quad (9)$$

Assume that the fracture area of coal per unit volume is  $S$

$$S = \pi b L_a \quad (10)$$

The fracture porosity can be expressed as

$$\varphi = \frac{bS}{2L^3} \quad (11)$$

Substituting equation (10) into equation (11), the fracture aperture can be written as

$$b = \sqrt{\frac{2\varphi L^3}{\pi L_a}} \quad (12)$$

Substituting equations (9) and (12) into equation (6), the fracture permeability can be rewritten as

$$k = \frac{\sqrt{2} L^{\frac{7}{2}} \varphi^{\frac{5}{2}m-1}}{6\pi^{\frac{3}{2}} a^{\frac{5}{2}}} \quad (13)$$

Here, the fracture model is presented in a cubic unit. Where the length and lithology index values are constant, the fracture permeability expression can be simplified as

$$k = c \varphi^{\frac{5}{2}m-1} \quad (14)$$

where  $c$  is a constant.

This model firstly introduced the cementation index ( $m$  value) and fracture porosity into the fracture permeability, which can finely describe the controlling factors of fracture permeability.

### Fracture porosity

The fracture porosity is very important to verify the accuracy of the model. This paper uses 3D finite element method combined with logging data to obtain fracture porosity of the regional CBM reservoirs.

**Fracture performance.** The fracture dip states can be divided into low-dip fractures, medium inclined fractures, and high-dip fractures using the deep lateral and shallow lateral

**Table 1.** Fracture state and assignment of fracture state coefficient.

Value	Status	$A_1$	$A_2$	$A_3$
$Y > 0.1$	High-dip fracture	8.522532	-8.242788	$7.1236 \times 10^{-4}$
$0 < Y < 0.1$	Medium inclined fracture	-17.6332	20.36451	$9.3177 \times 10^{-4}$
$Y < 0$	Low-dip fracture	-0.992417	1.97247	$3.18291 \times 10^{-4}$

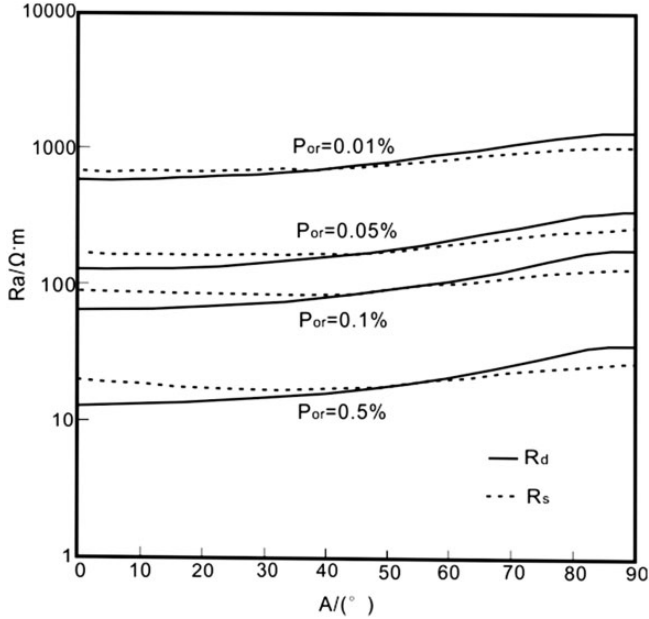


**Figure 3.** Effect of fracture inclination on dual laterolog.

logging data. The angle ranges are  $[0^\circ, 50^\circ]$ ,  $[50^\circ, 74^\circ]$ , and  $[74^\circ, 90^\circ]$ , respectively.

$$Y = (R_d - R_s) / \sqrt{R_d * R_s} \tag{15}$$

With reference to Figure 2 and equation (15), the relationship between  $Y$  and the angle of inclination of the fracture can be determined (Table 1).

The effect of fracture dip on dual lateral log response through extensive data (Li et al., 1996) has been summarized as shown in Figure 3.  $R_a$  is the apparent resistivity,  $A$  is the fracture dip, and  $P_{or}$  is the fracture porosity. For the CBM reservoirs in the SJB, the dual lateral logging response is a positive difference in the high-angle fracture state.

**Calculation of fracture porosity.** When determining the dip angle belongs to a certain fracture state, the approximate inversion formula of the dual lateral logging response is

$$\sigma_d = (d_1 + d_2x) + (d_3 + d_4x)\sigma_b \tag{16}$$

$$\sigma_s = (s_1 + s_2x) + (s_3 + s_4x)\sigma_b \tag{17}$$

$$x = \varphi_f \sigma_m \quad (18)$$

where  $\sigma_d$ ,  $\sigma_s$ ,  $\sigma_b$ , and  $\sigma_m$  represent the deep lateral conductivity, shallow lateral conductivity, original reservoir conductivity, and mud conductivity, respectively;  $d_1$ ,  $d_2$ ,  $d_3$ ,  $d_4$ ,  $s_1$ ,  $s_2$ ,  $s_3$ , and  $s_4$  are the coefficients. Although the original reservoir resistivity is uncertain, for a certain dip angle  $A$  reservoir resistivity should be a constant. Substituting equation (16) into equation (17), the  $x$  can be rewritten as

$$x = A_1 \sigma_s + A_2 \sigma_d + A_3 \quad (19)$$

where  $A_1$ ,  $A_2$ , and  $A_3$  are the coefficients.

Based on the 3D finite element method, the values for different dip angles  $A_1$ ,  $A_2$ , and  $A_3$  are presented as shown in Table 1.

First, we need to correct the mud resistivity in the formation. As the burial depth of the coal seam increases, the temperature rises and the resistivity of the drilling fluid decreases. Take Well-7 as an example, the resistivity of drilling fluid configured at 25°C is 1.96, which corresponds to the resistivity of drilling fluid at 18°C

$$R_{m(18)} = R_m(1 + 0.023 * (t_1 - 18)) = 2.2756 \Omega \cdot m \quad (20)$$

The bottom temperature of the target coal seam is 21.96°C, and the resistivity of the target coal seam drilling fluid is

$$R_{m_f} = R_{m(18)} / (1 + 0.023(t_2 - 18)) = 2.0856 \Omega \cdot m \quad (21)$$

The fracture-related parameters of coal reservoirs in the Fukang area of the southern margin of the Junggar Basin are shown in Table 2. From Table 2, it can be seen that the regional development is inclined and high-angle coal seams, the fracture porosity is between 1‰ and 25‰.

### Formation cementation index ( $m$ value) by fractal methods

*Fractal characteristics of well logging curves.* The formation (fracture) cementation index ( $m$  value) can reflect the difficulty of fluid flow through a fracture or reservoir. Generally, the  $m$  value increases as the fracture curvature increases. When the fluid flows through long and curved fractures, that is, densely populated fracture areas, the  $m$  value is large (typically 1.8–2.2). When the fluid flows through a short and straight fracture, the value of  $m$  could take the minimum (ideally 1.0) as shown in Figure 4. To accurately determine the reservoir resistivity, a high accuracy of formation cementation index  $m$  is required. Logging curves can continuously record the petrophysical parameters with ongoing drilling. The fractures can be reflected by the logging curves. The permeability of the formations at different scales has a similar distribution when they have the same complexity due to the self-similar structures in these complex formations. The logging curve is an indirect reflection of the physical property of the formation including the fracture features. The fractal dimension of the logging curve can be calculated using the



**Table 2.** Well logging data and fracture porosity of coalbed methane reservoir in the southern Junggar Basin.

Well	RLLD	RLLS	Rm	t <sub>2</sub>	Rmf	Y	φ <sub>f</sub> (10 <sup>-3</sup> )
W1	1351	433	0.37	35.79	0.26	1.201	3.754
W2	9113	8514	1.4	19	1.37	0.068	1.518
W3	403	450	2.5	20.32	2.38	-0.108	7.122
W4	292	296	0.51	25.4	0.51	-0.013	1.881
	5514	1551	0.51	28.32	0.48	1.355	2.254
W5	165	142	0.43	20.17	0.48	0.153	5.208
	216	162	0.43	21.24	0.46	0.289	7.041
	300	242	0.43	24.09	0.44	0.216	3.716
W6	394	334	0.41	31.23	0.36	0.166	1.929
W7	957	993	1.96	21.96	2.09	-0.037	2.88
W8	216	186	2.34	16.25	2.83	0.151	23.812
	413	361	2.34	18.55	2.68	0.135	11.703
	336	316	2.34	23.6	2.41	0.063	13.639
W9	8701	428	1.62	35	1.16	2.271	20.834
W10	2295	2319	0.94	24.09	0.82	-0.010	0.618
W11	966	601	0.32	25.1	0.28	0.480	1.753

Note: RLLD is the deep lateral resistivity, Ω-m; RLLS is the shallow lateral resistivity, Ω-m; Rm is the mud resistivity configured at a specific temperature, Ω-m; t<sub>2</sub> is the formation temperature, °C; Rmf is the corrected mud resistivity, Ω-m; Y is the crack state. φ<sub>f</sub> is the fracture porosity, %.

embedded space method (Shi and Pan, 2000; Wang et al., 1998; Yang et al., 2006). The specific steps are as follows:

- (1) Establishing phase space. If there are *n* data points, the data sequence of a logging curve are (x<sub>1</sub>, x<sub>2</sub>, . . . , x<sub>n</sub>). The establishment of vector space into *N* groups of data ( $\vec{Y}_1, \vec{Y}_2, \vec{Y}_3, \dots, \vec{Y}_n$ ), each vector comprising a space dimension *u*. The truncated *u* data constitutes one vector of the phase space. And one (or *A*) data is moved backward to intercept *u* data, which in turn constitutes another vector. Interception is performed on a well log curve at regular intervals to obtain the corresponding expansion data sequence

$$\begin{aligned}
 &\vec{Y}_1(x_1, x_2, x_3, \dots, x_u) \\
 &\vec{Y}_2(x_{1+A}, x_{2+A}, x_{3+A}, \dots, x_{u+A}) \\
 &\vec{Y}_3(x_{1+2A}, x_{2+2A}, x_{3+2A}, \dots, x_{u+2A}) \\
 &\vdots \\
 &\vec{Y}_i(x_{1+(i-1)A}, x_{2+(i-1)A}, x_{3+(i-1)A}, \dots, x_{u+(i-1)A}) \\
 &\vdots \\
 &\vec{Y}_N(x_{1+(N-1)A}, x_{2+(N-1)A}, x_{3+(N-1)A}, \dots, x_{u+(N-1)A})
 \end{aligned} \tag{22}$$

where *i* = 1, 2, . . . , *N*. The one-dimensional space of the time series is presented to the *u*-dimensional phase space.

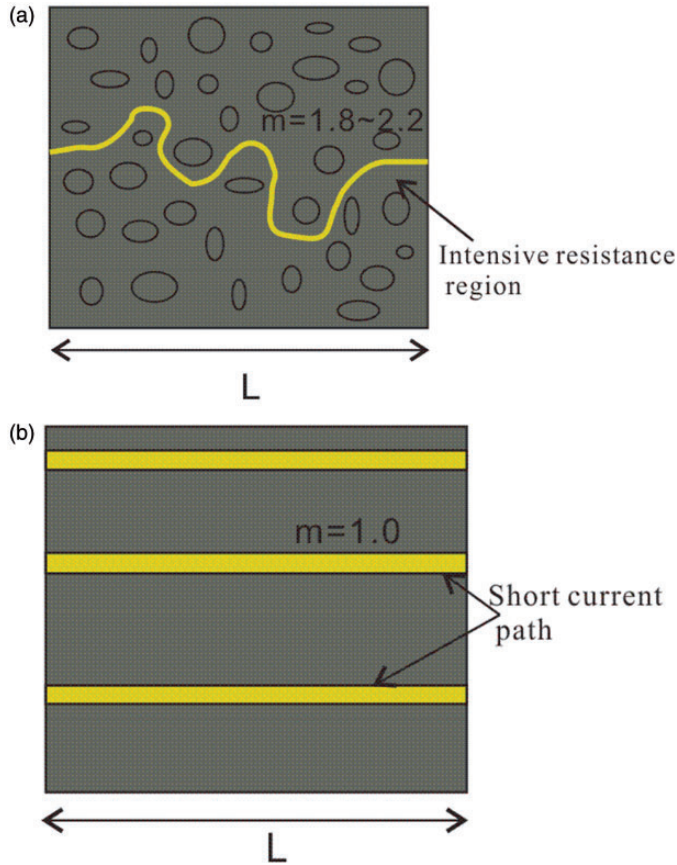


**Figure 4.** Core currents with different cementation levels.

- (2) Calculating the Euclidean distance between points in phase space. For any two vectors in the embedding space, such as  $\vec{Y}_i, \vec{Y}_j (i, j = 1, 2, 3, \dots, N)$ , the distance between them is

$$R_{ij} = |\vec{Y}_i - \vec{Y}_j| = \sqrt{\sum_{c=1}^m (x_{c+(i-1)A} - x_{c+(j-1)A})^2} \quad (23)$$

where  $i \neq j$ .

- (3) Statistical  $R_{ij}$  at different scales. For a given scale  $\epsilon$ , the number of distances satisfying the condition of  $R_{ij} < \epsilon (i \neq j)$  is  $S(\epsilon)$ . The total number is  $N^2$  for any two vector combinations. The ratio of the number of distances satisfying the conditions under this scale to the total number of distances is

$$C(\epsilon) = \frac{S(\epsilon)}{N^2} \quad (24)$$

(4) Calculating the fractal dimension  $D$ . The fractal dimension can be expressed as

$$D = \lim_{\varepsilon \rightarrow 0} \frac{\lg C(\varepsilon)}{\lg \varepsilon} \quad (25)$$

When the vector dimension  $u$  takes a value of 6 or more, the calculated correlation dimension is very stable. Therefore, for taking the length, according to the sampling rate of 8 sampling points per meter of the current logging curve, the length cannot be less than 1 m. Otherwise, the fractal dimension cannot be calculated.

**Determination of the  $m$  value.** In this work, the formation cementation index ( $m$  value) will be calculated by using the vector dimension  $U = 10$ . To make the scale  $\varepsilon$  have the ability to automatically select value,  $\varepsilon_1 = 1.1 \times \varepsilon_0$  ( $\varepsilon_0$  is the value of controlling  $C(\varepsilon_0) \approx 0.06$ ) is used to generate the sequence  $\varepsilon$ . The sequence  $C(\varepsilon)$  value is obtained. If choosing the appropriate sequence  $\varepsilon$ , there are

$$C(\varepsilon) \propto \varepsilon^D \quad (26)$$

$$\log C(\varepsilon) \propto D \log \varepsilon \quad (27)$$

Line segments can be expressed as

$$\log C(\varepsilon) = D \log \varepsilon + A \quad (28)$$

where  $D$  is the slope of the line, which is the fractal dimension;  $A$  is the intercept of the line segment.

AC, CNL, and DEN can reflect the pore structure of the formation. If the fractal dimensions for AC, CNL, and DEN are  $D_{AC}$ ,  $D_{CNL}$ , and  $D_{DEN}$ , respectively, the fractal dimension of the formation cementation index ( $m$  value) is named  $D_m$ . According to the fractal dimension of the three logging curves, the scholars used the factor analysis method to obtain the coefficient relationship, and compared with the experimental values, the results are more consistent and meet the basic requirements of the analysis. In this area, the fractal dimension of the well log is obtained. Using the same method, the ratio of the coefficients is approximately 2:1:1. Therefore, this method can be used for analysis. The  $D_m$  has a strong linear correlation with the formation cementation index ( $m$  value) (Li et al., 1996)

$$D_m = [(D_{CNL} + D_{DEN}) + 2 \cdot D_{AC}] / 4 \quad (29)$$

For instances, the AC, CNL, and DEN data of the corresponding A5 coal seam are selected from the Well W1. Using above equation (28), the fractal dimensions can be calculated. There are 65 logging data points in the coal seam. To improve the accuracy of the results, the step length is set to be 1 to establish the vector space. Then the relationship between  $\log C(\varepsilon)$  and  $\log \varepsilon$  can be established.

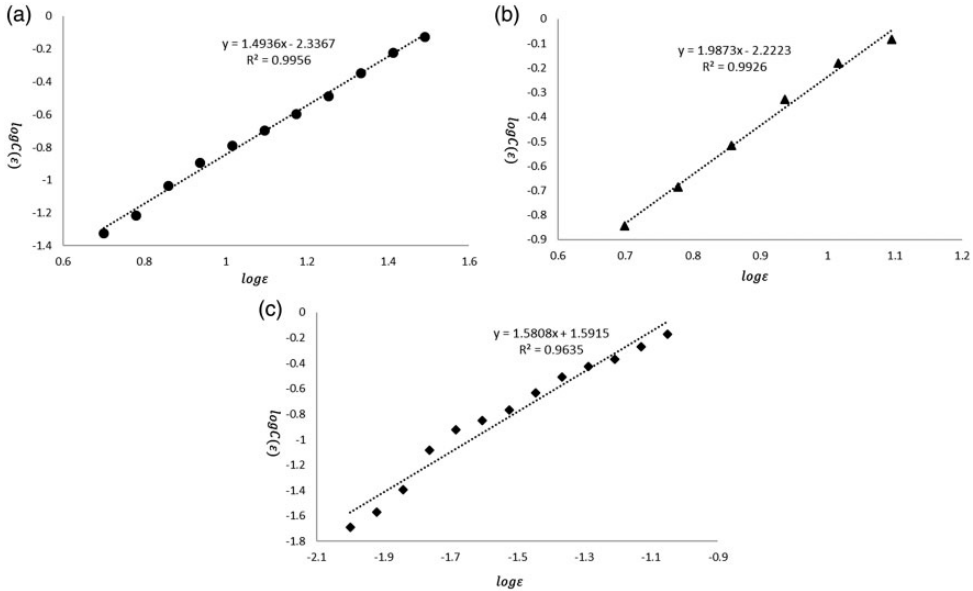


**Figure 5.** Fractal dimension fitting lines of different well logging curves. (a) Acoustic logging fractal dimension fitting line, (b) compensated neutron logging fractal dimension fitting line, and (c) density logging fractal dimension fitting line.

As shown in Figure 5(a), the fractal dimension of AC is 1.4936. Similarly, the CNL and DEN fractal dimensions are 1.9873 and 1.5808, respectively (Figure 5(b) and (c)). The fractal dimension of the formation cementation index of the A5 coal seam in well W1 is 1.638825. Compared with the formation cementation index obtained by rock electricity experimental test, the value using the fractal method through the geophysical logging includes the CBM reservoir heterogeneity, which can provide a more accurate value closer to the real CBM reservoir. Therefore, the fractal dimension of the formation cementation index of the other coal seams is normally distributed between 1.2 and 1.9.

### Model validation and high-dip fracture permeability prediction

In Figure 6(a), a fitted relationship is established by using the fracture porosity and the well test permeability. Currently, the fracture permeability is proportional to the cubic of fracture porosity. Figure 6(b) shows that the fracture permeability and the fracture cubic porosity show a good correlation in the CBM reservoir of the SJB. To perform the logarithm of equation (14), the CBM reservoir permeability of the coal is expressed as

$$\ln k \propto \left( \frac{5}{2}m - 1 \right) \ln \phi_f \tag{30}$$

According to equation (30), the correlation line between them can be established as shown in Figure 7. For CBM reservoirs in the SJB, the original permeability is measured by the well testing, which can reflect the comprehensive permeability of the CBM reservoir.

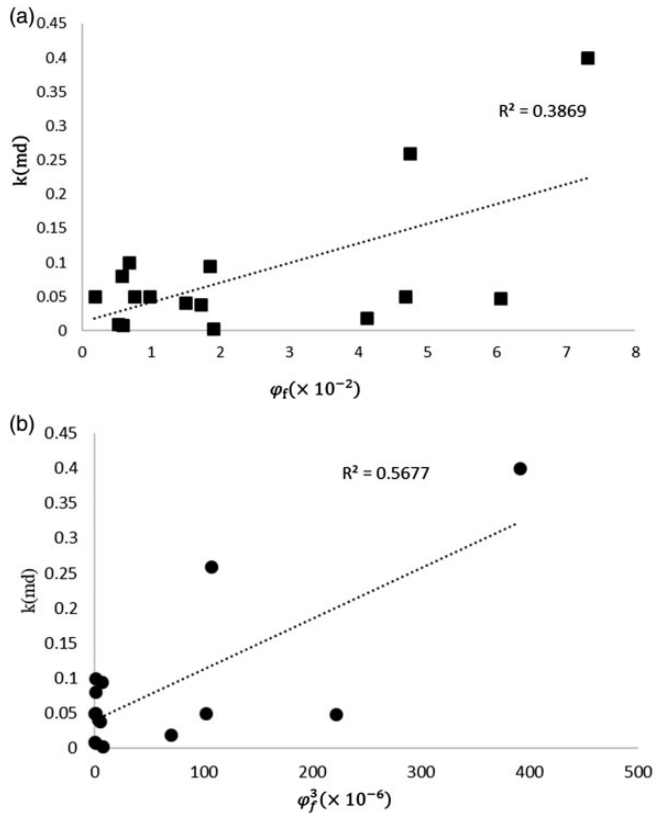


**Figure 6.** The relationships between fracture porosity,  $\phi_f^3$  and the permeability of test well. (a) The relationship between fracture porosity and the permeability of test well; (b) the relationship between  $\phi_f^3$  and the permeability of test well.

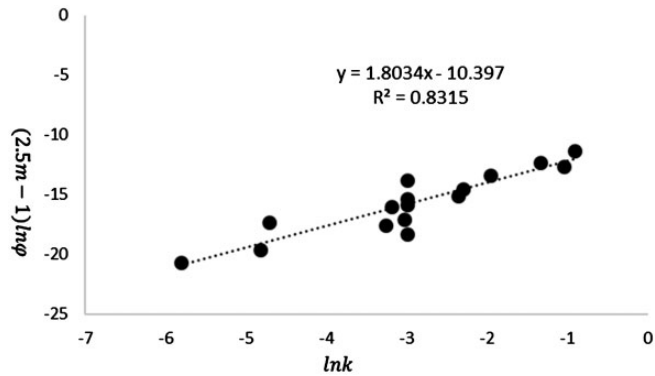


**Figure 7.** The relationship between the permeability of the model and the permeability of test well.

**Table 3.** Original parameters of coal reservoir in the southern Junggar basin.

Well	$\varphi_f (10^{-3})$	m	$k(md)$	$lnk$	$(2.5m^{-1})ln\varphi_f$
W1	3.754	1.525	0.05	-2.99573	-18.266
W2	1.518	1.782	0.048	-3.03655	-17.0857
W3	7.122	1.519	0.038	-3.27017	-17.568
W4	1.881	1.686	0.008	-4.82831	-19.6057
	2.254	1.614	0.041	-3.19418	-15.9672
W5	5.208	1.481	0.14	-1.96611	-13.3974
	7.041	1.436	0.1	-2.30259	-14.4917
	3.716	1.722	0.003	-5.80914	-20.6724
W6	1.929	1.431	0.095	-2.35916	-15.081
W7	2.88	1.610	0.4	-0.91629	-11.3081
W8	23.812	1.783	0.05	-2.99573	-15.3832
	11.703	1.546	0.26	-1.34707	-12.311
	13.639	1.821	0.05	-2.99573	-13.7603
W9	20.834	1.638	0.009	-4.71053	-17.2969
W10	0.618	1.258	0.05	-2.99573	-15.8575
W11	1.753	1.197	0.35	-1.04982	-12.6499

**Table 4.** Predicted original high-dip fracture permeability of the coalbed methane reservoir.

Well	RLLD	RLLS	$\varphi_f(10^{-3})$	m	$k(md)$
W12	197.6115	175.743	4.751	1.54755	0.064265
W13	637.0831	628.5951	5.078	1.654475	0.032655
	2468.351	1498.578	3.187	1.853175	0.002981
	840.3619	773.9346	2.447	1.7674	0.00358
W14	643.5307	599.5862	3.627	1.6057	0.026594
	2671.551	1716.444	2.957	1.69665	0.00907
W15	1416.645	632.4151	6.068	1.6078	0.06192
	253.6067	272.3821	3.158	2.1276	0.000327
W16	1038.085	1023.866	1.926	1.976525	0.000371
	1790.367	1353.15	1.382	1.9397	0.000251
W17	151.9463	101.763	18.858	1.6233	0.379632
W18	526.3326	290.147	11.178	1.5866	0.196549
W19	357.3441	347.9555	9.044	1.807375	0.032862
	192.5594	198.3738	6.908	1.9236	0.008715
	232.7805	243.7512	5.849	1.943875	0.005308
W20	259.6933	264.5244	3.493	1.742525	0.008538
W21	141.1221	180.6684	20.141	1.7922	0.170119
	326.94	271.8523	15.352	1.77895	0.108759
	839.9478	674.1568	6.978	1.68585	0.04573
	4368.241	995.8639	13.952	1.730225	0.120894
W23	92.63686	101.5141	9.012	2.0098	0.008705
	315.6703	275.9209	4.082	2.020375	0.001371
	702.251	505.3412	4.187	2.138775	0.000591
W24	186.5877	137.085	10.729	1.86284	0.03236

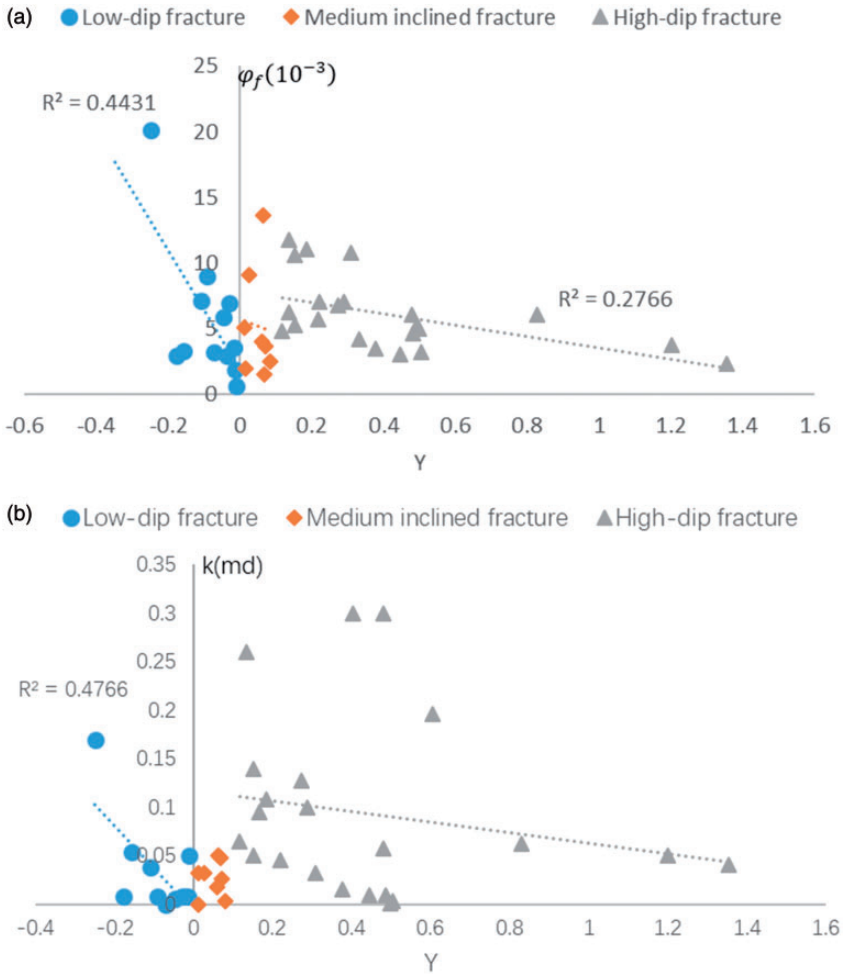


**Figure 8.** The relationships between coal reservoir permeability, fracture porosity, and dip angle. (a) Relationship between dip angle and fracture porosity; (b) relationship between dip angle and coal reservoir permeability.

The calculated permeability of this model and the measured permeability by well testing are shown in Table 3. In Table 3, the derived fracture porosity and formation cementation index values are brought into equation (30) to obtain the value of  $(2.5m-1)\ln\phi_f$ .  $\ln k$  is the logarithmic value of actual well test permeability. From Table 3, the fracture porosity and formation cementation index of the CBM reservoir in the study area vary greatly, and the plane heterogeneity is relatively strong, which indicates variable fracture permeability.

As shown in Figure 7, the calculated permeability fitted well with results from the well testing ( $R^2=0.8315$ ), which indicates that the model can be used to accurately predict the original formation permeability of coal reservoirs in the southern margin of the Junggar Basin. The mathematical fracture permeability is proportional to the cube of the fracture

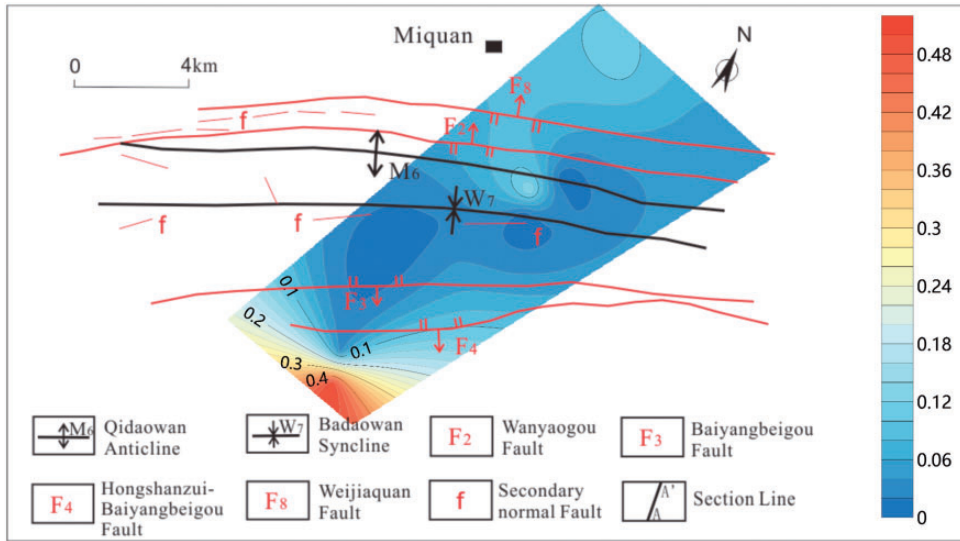


**Figure 9.** The no. 43 seam permeability distribution by the established high-dip fracture permeability model.

porosity. Here, the formation cementation index introduced in this model shows strong superiority and accuracy. The equation (30) can be rewritten as

$$\left(\frac{5}{2}m - 1\right) \ln \phi_f = 1.8034 \ln k - 10.397 \tag{31}$$

Due to the limited well testing permeability in the SJB, the established permeability model was used to evaluate the CBM reservoir permeability in Hedong mining area of the SJB. The equation (31) is obtained by using the well testing permeability of the CBM reservoir in the study area. Therefore, the fracture permeability can be rewritten as

$$k = e^{\frac{\left(\frac{5}{2}m - 1\right) \ln \phi + 10.397}{1.8034}} \tag{32}$$

The final application of equation (32) yields the corresponding fracture permeability of the CBM reservoir (Table 4). In the Table 4, the fracture permeability of coal reservoirs in the SJB is generally low. The relationship between the fracture porosity, the original permeability and the dip angle are established as shown in Figure 8. When the fracture develops at a low angle, the fracture porosity and the original permeability of the CBM reservoir should decrease as the angle increases. When the fractures develop in an inclined state, the fracture porosity and permeability values are disorganized and no obvious change trend due to the scarce data points. When fractures develop at high angles, fracture porosity and permeability of coal reservoirs decrease with increasing dip angle, which may need more works. The reservoir permeability of the No. 43 coal seam in the SJB is predicted as shown in Figure 9. Horizontally, the permeability of the No. 43 coal seam changed drastically.



The permeability change of the No. 43 coal seam showed a downward trend first and then increased from the south to the north part in the SJB. In the study area, the permeability of the CBM reservoir is 0.005–5 mD. In general, the area near the Hongshanzui-Bayangbeigou fault is the high-permeability zone of the No. 43 coal seam, whereas the center of the Yadaowan syncline is the low-permeability zone, which indicates that the local geological structure could be the main factor that causing the permeability variation in the plane.

## Conclusions

In this work, a new model for fracture permeability in a CBM reservoir is established with the combination of the  $m$  value (formation cementation index), the fracture porosity and the total porosity of the coal reservoir through the 3D finite element method. Then, the cementation index  $m$  value of CBM reservoir is detailed evaluated by the fractal dimensions from the well logging of AC, CNL, and DEN. Finally, the predicted permeability is calculated with the established fracture permeability model, which may indicate the complex geological structure for the CBM reservoir in the southern Junggar Basin, NW China. The main conclusions can be made:

1. The high-dip fracture porosity of CBM reservoirs was obtained by 3D finite element method, which ranges from 0.618% to 20.834%. The reservoir temperature can affect the accuracy of fracture porosity. AC, CNL, and DEN can effectively reflect the pore structure of CBM reservoirs. The formation cementation index  $m$  is calculated based on the logging data of AC, CNL, and DEN combining with fractal method.
2. Comparing the permeability from established model and well test, there is a perfectly linear correlation between them (correlation coefficients is 0.83). Therefore, the original permeability of the CBM reservoir obtained by the established model can accurately reflect the original permeability of the high-dip angle CBM reservoir in the southern Junggar Basin, NW China.
3. The reservoir permeability of the No. 43 high-dip angle CBM reservoir in the SJB changes drastically (0.005–5 mD). The permeability change of the No. 43 coal seam showed a downward trend first and then increased from the south to the north part in the SJB. The area near the Hongshanzui-Bayangbeigou fault is the high permeability zone, whereas the center of the Yadaowan syncline has low permeability, which indicates that the geological structure could be the main factor for causing the regional permeability variation.


## Declaration of conflicting interests

The author(s) declared no potential conflicts of interest with respect to the research, authorship, and/or publication of this article.

## Funding

The author(s) disclosed receipt of the following financial support for the research, authorship, and/or publication of this article: This research was funded by the National Major Research Program for Science and Technology of China (2016ZX05043-001), the National Natural Science Fund of China (grant nos. 41602170 and 41772160), the Royal Society International Exchanges-China NSFC Joint Project (grant nos. 4161101405 and RG13991-10), and Key Research and Development Projects of the Xinjiang Uygur Autonomous Region (2017B03019-01).

**ORCID iD**

Yidong Cai  <http://orcid.org/0000-0002-4915-5615>

**References**

- Cai Y, Liu D, Mathews JP, et al. (2014) Permeability evolution in fractured coal – Combining triaxial confinement with X-ray computed tomography, acoustic emission and ultrasonic techniques. *International Journal of Coal Geology* 122: 91–104.
- Cai Y, Liu D, Pan Z, et al. (2013) Pore structure and its impact on CH<sub>4</sub> adsorption capacity and flow capability of bituminous and subbituminous coals from Northeast China. *Fuel* 103: 258–268.
- Cai Y, Liu D, Yao Y, et al. (2011) Geological controls on prediction of coalbed methane of No.3 coal seam in Southern Qinshui Basin, North China. *International Journal of Coal Geology* 88: 101–112.
- Chatterjee R and Pal PK (2010) Estimation of stress magnitude and physical properties for coal seam of Rangamati area, Raniganj coalfield, India. *International Journal of Coal Geology* 81(1): 25–36.
- Chatterjee R and Paul S (2013) Classification of coal seams for coal bed methane exploitation in central part of Jharia coalfield, India – A statistical approach. *Fuel* 111: 20–29.
- Chen T, Wei D, Yang H, et al. (2006) The tectonic characteristics on the foreland thrust belt and its influence on reservoiring of oil and natural gas in Southern Junggar Basin. *Natural Gas Geosciences* 5: 711–718.
- Chen Z, Meng Z and Zeng L (2017) Formation mechanism and enrichment patterns of middle-low rank coalbed methane in Southern Junggar Basin, China. *China Coal Society* 42(12): 3203–3211.
- Clarkson CR, Rahmanian M, Kantzas A, et al. (2011) Relative permeability of CBM reservoirs: Controls on curve shape. *International Journal of Coal Geology* 88(4): 204–217.
- Connell LD (2016) A new interpretation of the response of coal permeability to changes in pore pressure, stress and matrix shrinkage. *International Journal of Coal Geology* 162: 169–182.
- Connell LD, Mazumder S, Sander R, et al. (2016) Laboratory characterisation of coal matrix shrinkage, cleat compressibility and the geomechanical properties determining reservoir permeability. *Fuel* 165: 499–512.
- Espinoza DN, Pereira JM, Vandamme M, et al. (2015) Desorption-induced shear failure of coal bed seams during gas depletion. *International Journal of Coal Geology* 137: 142–151.
- Espinoza DN, Vandamme M, Pereira JM, et al. (2014) Measurement and modeling of adsorptive–poromechanical properties of bituminous coal cores exposed to CO<sub>2</sub>: Adsorption, swelling strains, swelling stresses and impact on fracture permeability. *International Journal of Coal Geology* 134: 80–95.
- Fu H, Tang D, Xu H, et al. (2016) Abrupt changes in reservoir properties of low rank coal its control factors for methane absorbability. *Energy & Fuels* 30: 2084–2094.
- Gensterblum Y, Merkel A, Busch A, et al. (2014) Gas saturation and CO<sub>2</sub> enhancement potential of coalbed methane reservoirs as a function of depth. *AAPG Bulletin* 98(2): 395–420.
- Gentzis T, Deisman N and Chalaturnyk RJ (2009) Effect of drilling fluids on coal permeability: Impact on horizontal wellbore stability. *International Journal of Coal Geology* 78(3): 177–191.
- Karacan CO, Ulerly JP and Goodman GVR (2008) A numerical evaluation on the effects of impermeable faults on degasification efficiency and methane emissions during underground coal mining. *International Journal of Coal Geology* 75(4): 195–203.
- Karacan CO, Ruiz FA, Cote M, et al. (2011) Coal mine methane: A review of capture and utilization practices with benefits to mining safety and to greenhouse gas reduction. *International Journal of Coal Geology* 86(2–3): 121–156.
- Kundu P, Kumar V and Mishra IM (2016) Experimental and numerical investigation of fluid flow hydrodynamics in porous media: Characterization of pre-Darcy, Darcy and non-Darcy flow regimes. *Powder Technology* 303: 278–291.
- Levine JR (1996) Model study of the influence of matrix shrinkage on absolute permeability of coal bed reservoirs. *Geological Society London Special Publications* 109(1): 197–212.

- Li G (2016) Coal reservoir characteristics and their controlling factors in the eastern Ordos basin in China. *International Journal of Rock Mechanics and Mining Sciences* 26: 1051–1508.
- Li JQ, Liu DM, Yao YB, et al. (2011) Evaluation of the reservoir permeability of anthracite coals by geophysical logging data. *International Journal of Coal Geology* 87: 121–127.
- Li S, Xiao C, Wang H, et al. (1996) Mathematical model of dual laterolog response to fracture and quantitative interpretation of fracture porosity. *Acta Geophys Sinica* 39(6): 845–852.
- Li Y, Yu X, Shan X, et al. (2017) The characteristics and mode of the braided-river delta of the Wulabo Formation of the Sigonghe section in the southern Junggar Basin. *Natural Gas Geosciences* 28(11): 1678–1688.
- Martin JM and Malone DH (2017) Three-dimensional modeling of Pennsylvanian sandstone units in the mature Dudley oil field, Illinois, USA. *Journal of Petroleum Exploration and Production Technology* 7(2): 433–449.
- Masoumi R, Calagari AA, Siahcheshm K, et al. (2017) Consideration of geological aspects and geochemical parameters of fluids in Bushdi geothermal field, south of mount Sabalan, NW Iran. *Journal of African Earth Sciences* 129: 692–700.
- Mitra A, Harpalani S and Liu S (2012) Laboratory measurement and modeling of coal permeability with continued methane production: Part 1 - Laboratory results. *Fuel* 94(1): 110–116.
- Ruspini LC, Farokhpour R and Oren PE (2017) Pore-scale modeling of capillary trapping in water-wet porous media: A new cooperative pore-body filling model. *Advances in Water Resources* 108: 1–14.
- Saboorian JH, Ashoori S and Mowazi G (2015) A new transient matrix/fracture shape factor for capillary and gravity imbibition in fractured reservoirs. *Energy Sources Part A-Recovery Utilization and Environmental Effects* 37(23): 2497–2506.
- Shi Y and Pan B (2000) The application of fractal: The quantitative description of features of fractures. *Geophysical and Geochemical Exploration* 6: 426–430.
- Shovkun I and Espinoza DN (2017) Coupled fluid flow-geomechanics simulation in stress-sensitive coal and shale reservoirs: Impact of desorption-induced stresses, shear failure, and fines migration. *Fuel* 195: 260–272.
- Vishal V (2017) Recent advances in coal seam sequestration research in India – Highlighting multi-phase CO<sub>2</sub> flow for deep seam sequestration. *Energy Procedia* 114: 5377–5380.
- Wang T, Xu L, Xu L, et al. (1998) Determining m and n values with fractal theory and its application. *Well Logging Technology* 1: 18–21.
- Winsauer W and Shearin H (1952) Resistivity of brine-saturated sands in relation to pore geometry. *AAPG Bulletin* 36(2): 253–277.
- Wyllie MR and Spangler MB (1952) Application of electrical resistivity measurement to problem of fluid flow in porous media. *AAPG Bulletin* 36(2): 359–403.
- Yan J, He X, Geng B, et al. (2017) Models based on fractal theory to assess pore structure of low permeability sand reservoirs. *Well Logging Technology* 41(3): 345–352.
- Yang Y, Peeters M and Cloud TA (2006) Gas productivity related to cleat volumes derived from focused resistivity tools in coalbed methane (CBM) fields. *Petrophysics* 47: 250–257.
- Yin H (2009) Prospect of exploration of CBM resources in Fukang coal mining area in Xinjiang and recommendations on its development. *China Coalbed Methane* 6(2): 16–18.
- Zheng B and Li J (2015) A new fractal permeability model for porous media based on Kozeny-Carman equation. *Natural Gas Geosciences* 26(1): 193–198.
- Zhou FD and Ya GD (2014) Sensitivity analysis in permeability estimation using logging and injection-falloff test data for an anthracite coalbed methane reservoir in Southeast Qinshui Basin, China. *International Journal of Coal Geology* 131: 41–51.